Initial Structural Models of the Aβ42 Dimer from Replica Exchange Molecular Dynamics Simulations

Nikolay Blinov,[*,†,‡] Massih Khorvash,[¶] David S. Wishart,[§] Neil R. Cashman,[¶] and Andriy Kovalenko[‡,†]

†*Department of Mechanical Engineering, University of Alberta, Edmonton, Alberta T6G 1H9, Canada*

‡*National Institute for Nanotechnology, National Research Council of Canada, Edmonton, Alberta T6G 2M9, Canada*

¶*Department of Medicine, University of British Columbia, Vancouver, British Columbia V6T 2B5, Canada*

§*Departments of Computing Science and Biological Sciences, University of Alberta, Edmonton, Alberta T6G 2E8, Canada*

E-mail: nblinov@ualberta.ca

Phone: +1 (780)641 1719. Fax: +1 (780) 641 1601

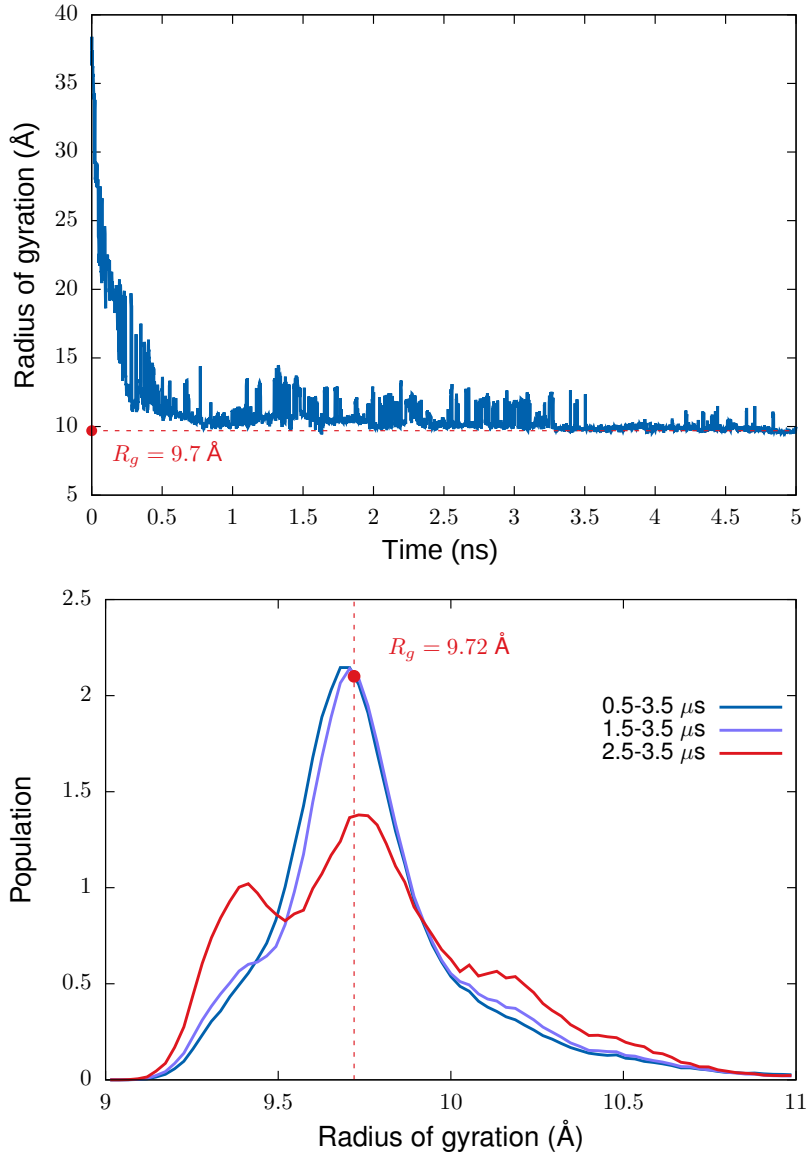

Figure S1: Top panel: time evolution of the radius of gyration of the Aβ42 monomer during the first 5 ns of the equilibration REMD run. The dashed line corresponds to the maximum of the radius of gyration distribution calculated for the first production segment of the trajectory (highlighted in Figures 1–3 of the main text). Bottom panel: Distribution of the radius of gyration for different parts of the trajectory. The red circle and dashed line indicate the radius of gyration value of 9.72 Å corresponding to the centroid structure of the most populated cluster from the first production segment of the trajectory identified with clustering of time series of the radius of gyration. This structure is used as a reference for RMSD calculations. Here and below all figures with the REMD data show results for the REMD replica corresponding to 25°C.

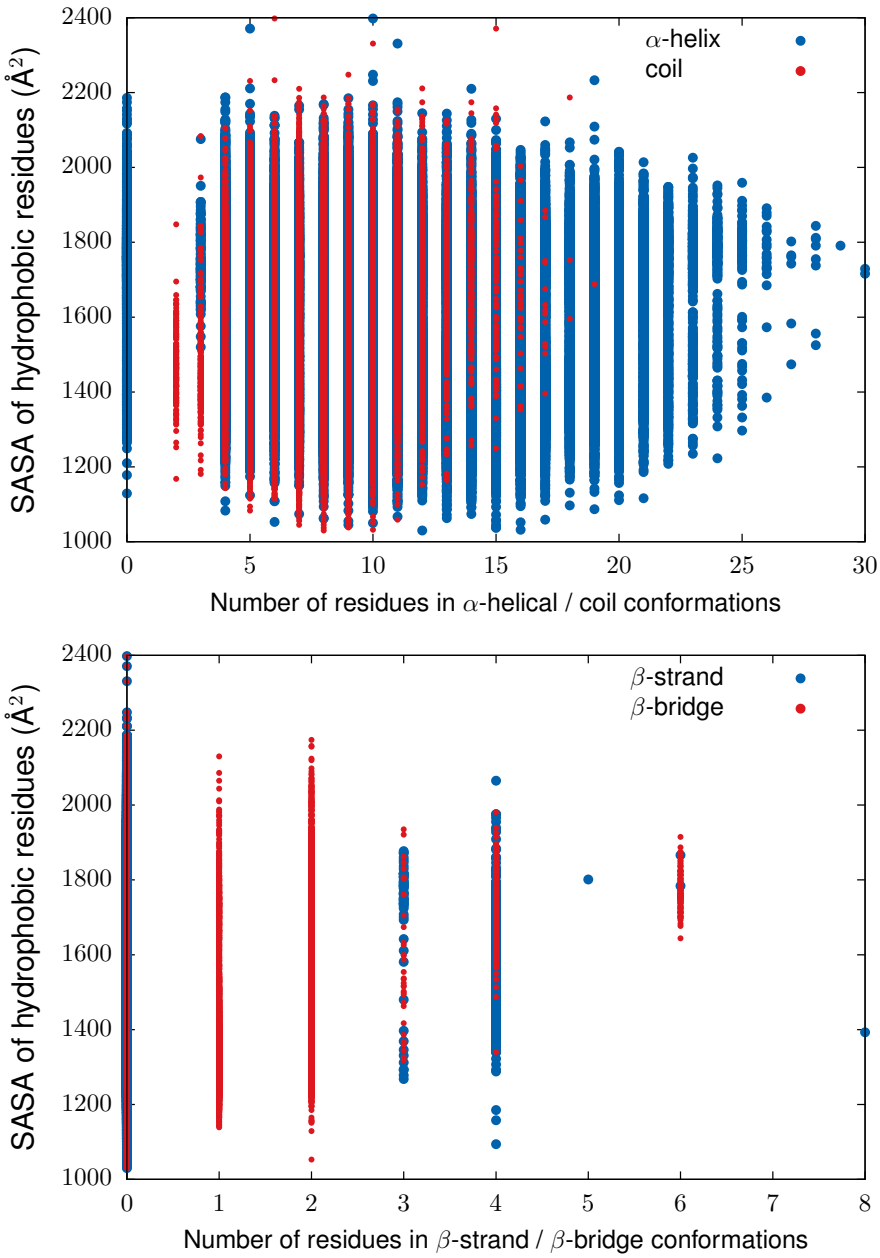

Figure S2: Solvent accessible surface area (SASA) of hydrophobic residues of the Aβ42 monomer plotted versus the number of residues forming different secondary structure elements: α-helices and coils (the top panel), β-strands and β-bridges (the bottom panel). The results are for the production part (the last 2μs) of the MD trajectory.

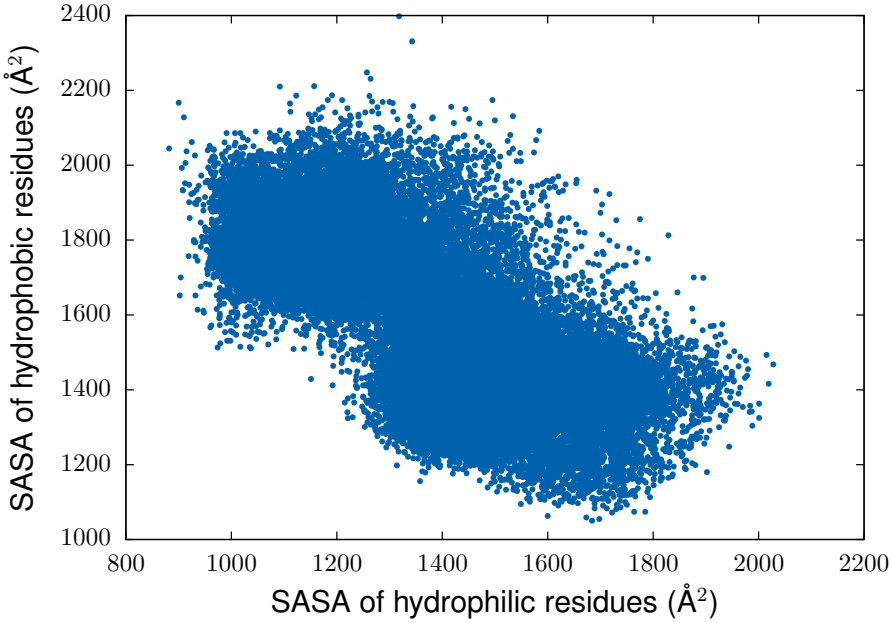

Figure S3: Solvent accessible surface area (SASA) of hydrophobic residues of the Aβ42 monomer plotted versus SASA of hydrophilic residues. The results are for the production part (the last 2μs) of the MD trajectory.

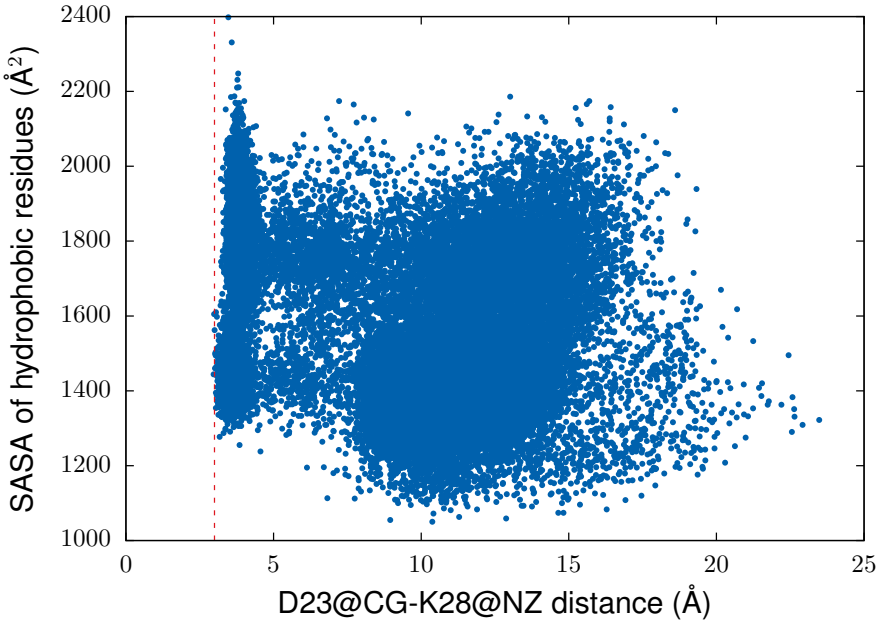

Figure S4: Solvent accessible surface area (SASA) of hydrophobic residues of the Aβ42 monomer plotted versus the distance between CG and NZ atomic sites of salt bridge-forming Asp23 and Lys28 residues. The results are for the production part (the last 2μs) of the MD trajectory.

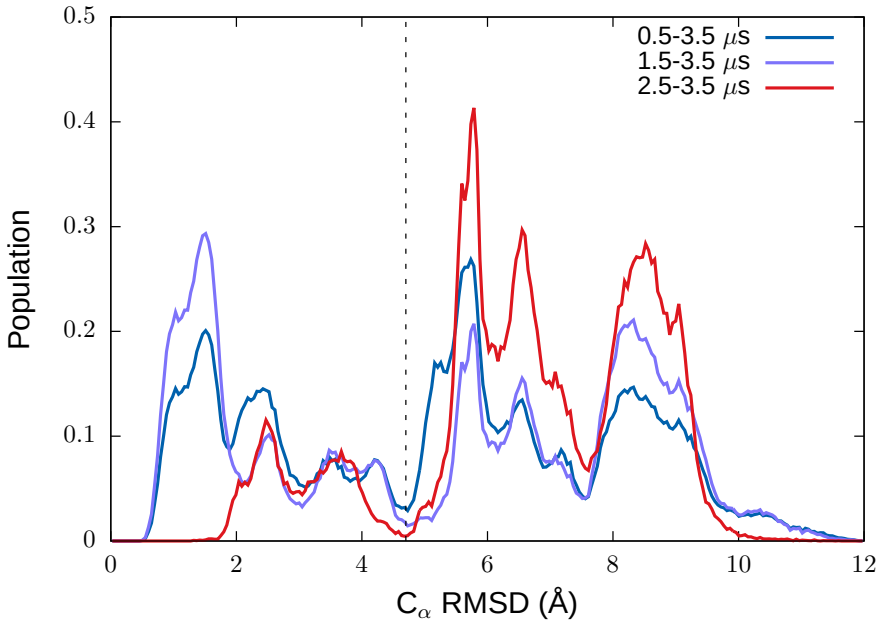

Figure S5: Population of the Cα RMSD values of the Aβ42 monomer calculated for the final 3 μs (blue color), 2 μs (violet color) and 1 μs (red color) intervals of the MD trajectory. The 1 μs interval includes the last production segment only, and the 2 and 3 μs intervals include both production segments of the trajectory with different propensity to form D23-K28 SB (as shown in Figure 1 of the main text). The vertical line at 4.7 Å tentatively separates the small and large RMSD domains.

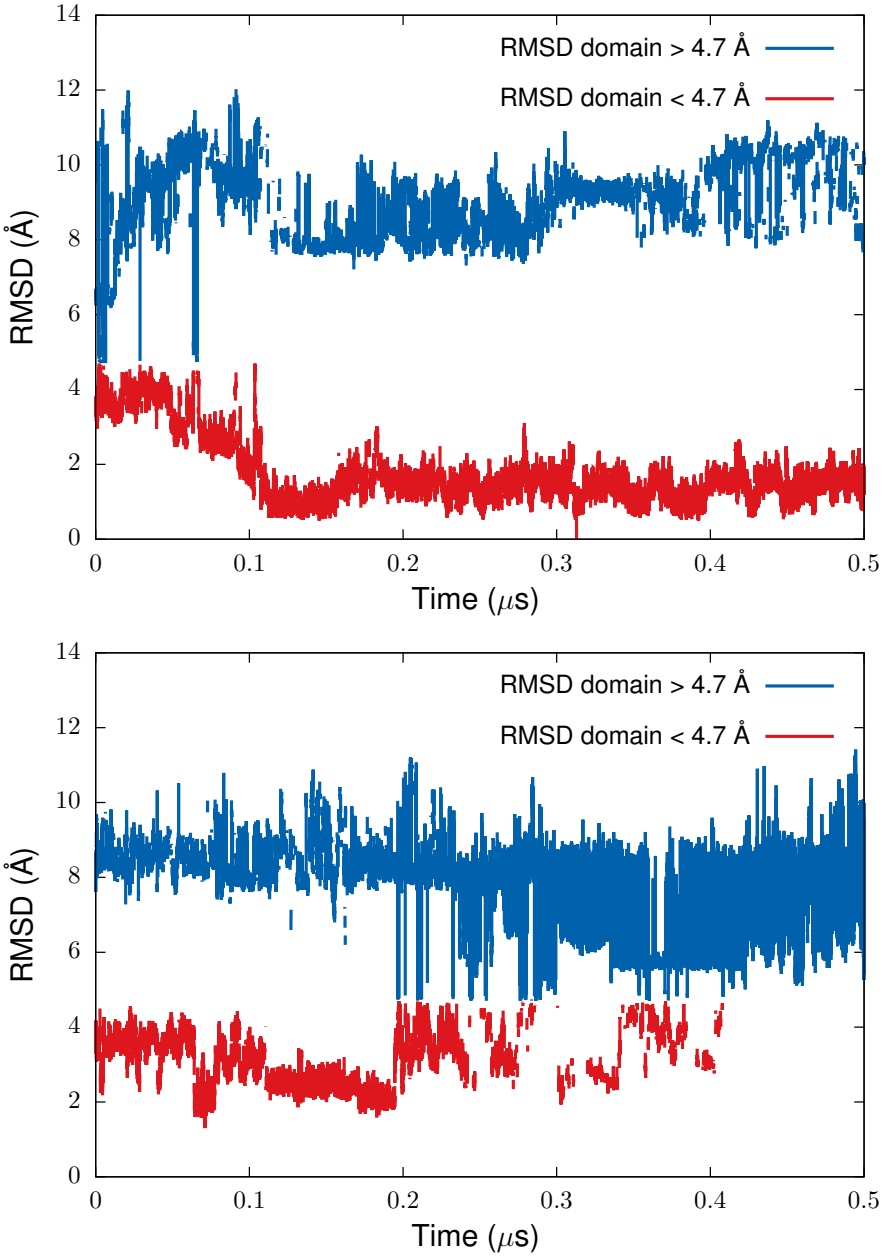

Figure S6: Time evolution of the Cα RMSD from the production REMD simulation of the Aβ42 monomer. As a reference for RMSD calculations, the centroid structure of the most populated cluster from clustering of time series of the radius of gyration was used. The RMSD values from the small and large RMSD domains are plotted in blue and red colors, respectively. The top and bottom panels are for two segments of the trajectory with different propensity to form D23-K28 SB (as indicated in Figure 1 of the main text).

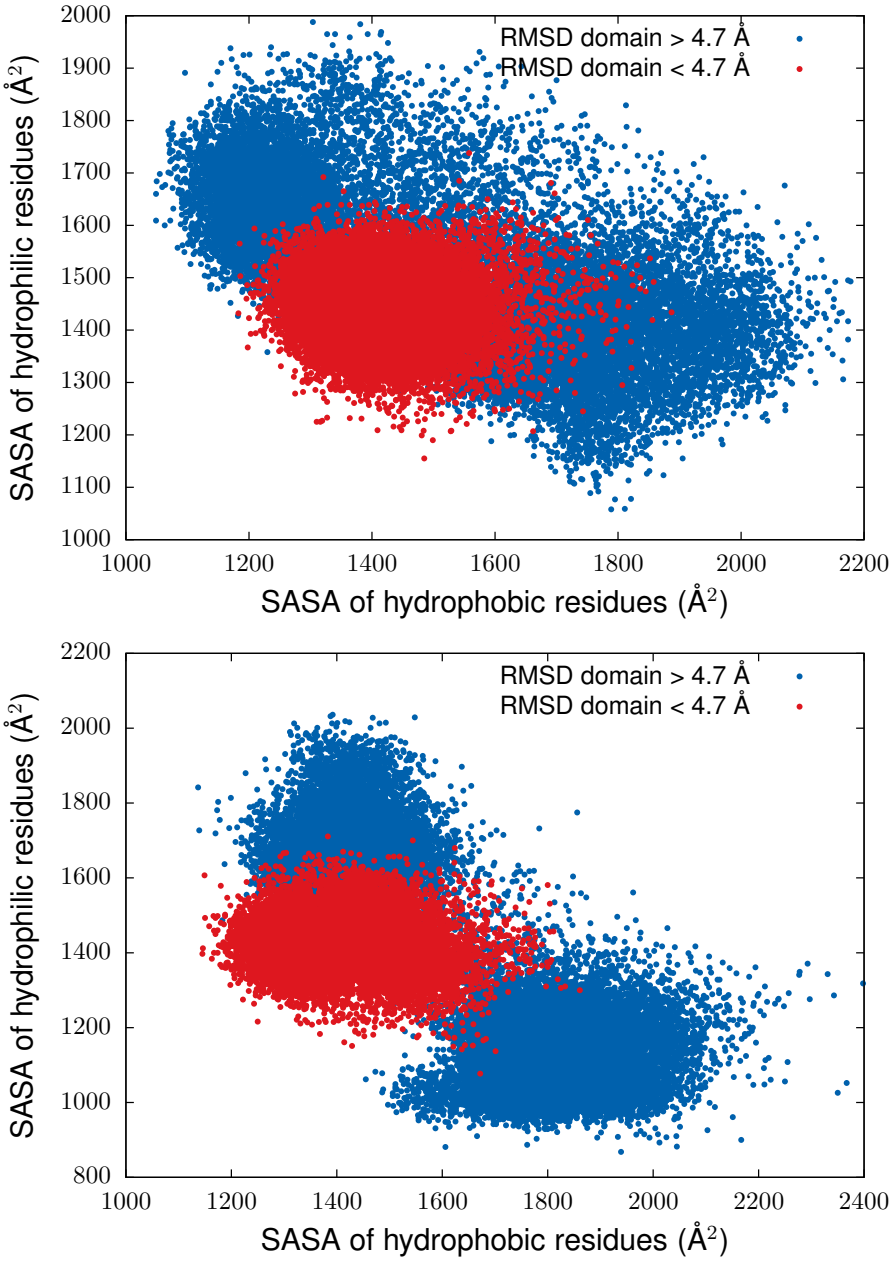

Figure S7: Distribution of solvent exposed surface area (SASA) of hydrophobic and hydrophilic residues of the Aβ42 monomer from the first (the upper panel) and the second (the bottom panel) production segments of the trajectory. Contributions from the large and small RMSD domains are shown with blue and red colors, respectively.

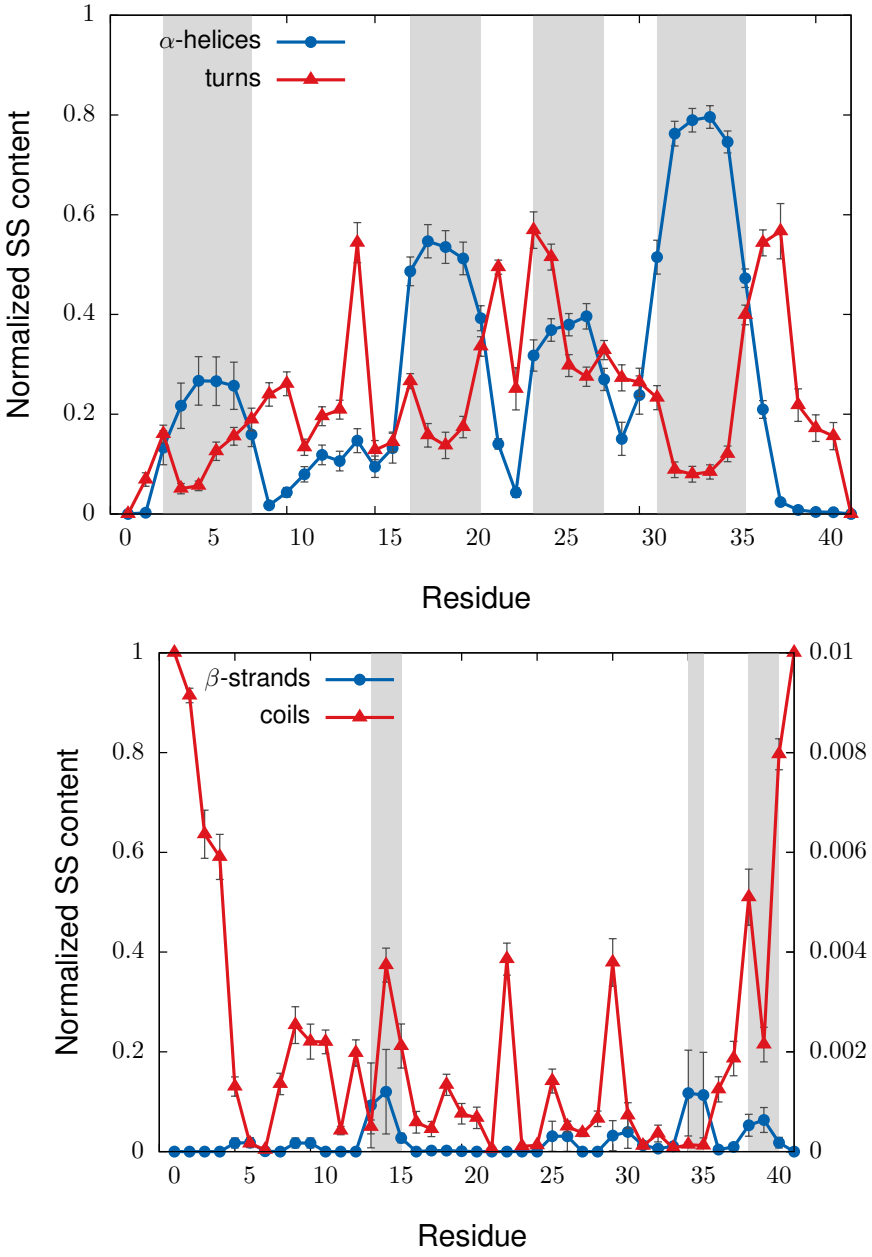

Figure S8: Per-residue secondary structure propensity of the Aβ42 monomer calculated for the final 2 μs part of the REMD trajectory. The average α-helical and turn content is shown in the top panel, and the β-strand and coil content in the bottom panel. The left and right axes in the bottom panel are for the coil and strand data, respectively. The gray areas highlight the ranges of residues with elevated α-helical (the top panel) and β-strand (the bottom panel) structures.

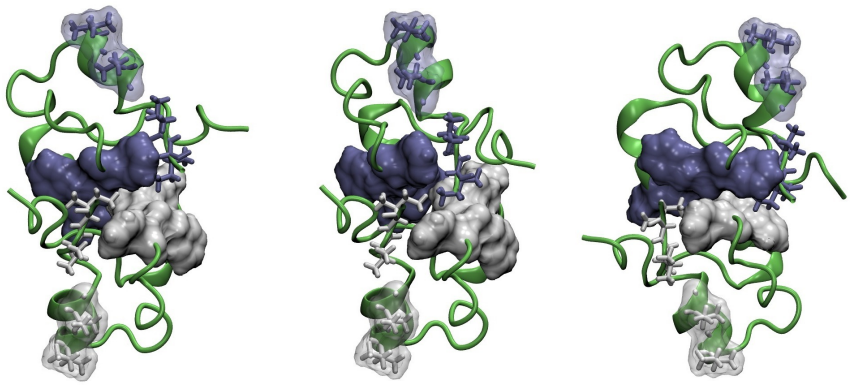

Figure S9: Three top-ranked models of the Aβ42 dimer built from the monomeric construct with a high solvent exposure of hydrophobic residues from the first production segment of the trajectory. First-, second-, and third-ranked structures are in the left, middle and right panels, respectively. Residues in the central hydrophobic cluster are shown by their molecular surface, hydrophobic Ile32, Val36, and C-terminal Val40 and Ile41 are shown in stick representation, with white and blue colors used for different monomers. For Ile32 and Val36 residues, transparent molecular surfaces are also shown.

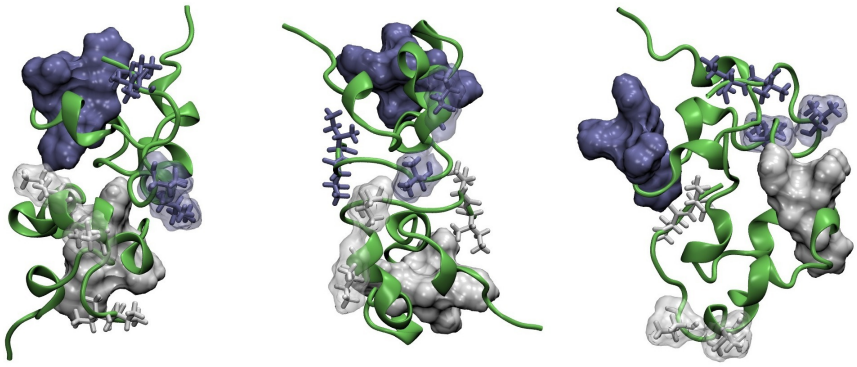

Figure S10: Same as in Figure S9 but for the last production segment of the trajectory.

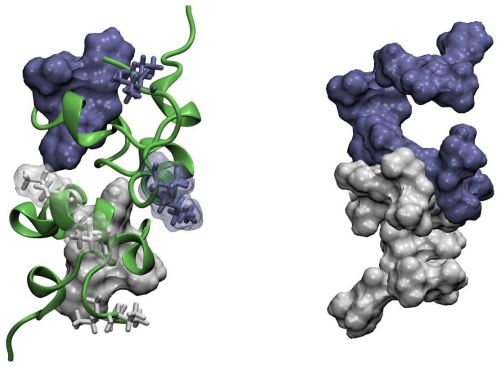

Figure S11: The first-ranked model of the Aβ42 dimer from Figure S10. On the left panel, residues in the central hydrophobic clusters are shown by their molecular surface, hydrophobic Ile32 and Val36 residues, as well as C-terminal Val40 and Ile41 are shown in stick representation, with white and blue colors used for different monomers. Transparent molecular surfaces of Ile32 and Val36 are also shown. On the right panel, molecular surfaces of hydrophobic residues (Ala, Leu, Val, Ile, Pro, Phe, Met, Trp) of the two constituting monomers are shown with different colors to illustrate a shape complementarity of the inter-peptide hydrophobic interface.

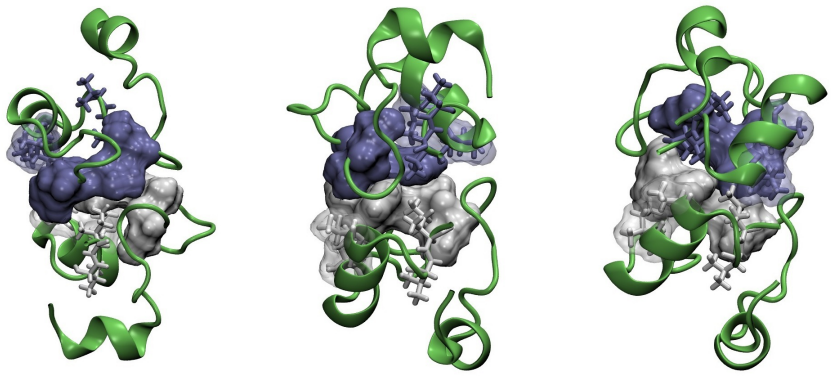

Figure S12: Three top-ranked models of the Aβ42 dimer built from the monomeric construct representing the most populated cluster from the first production segment of the trajectory. The same notations are used as in Figure S9.

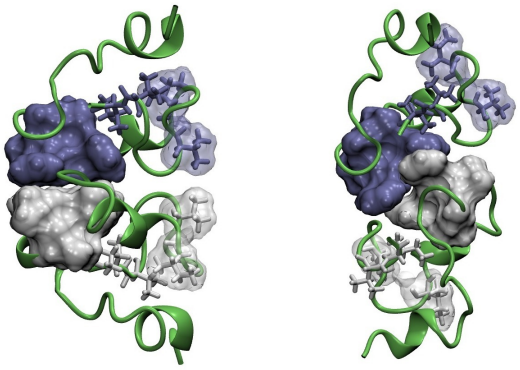

Figure S13: Two models of the Aβ42 dimer ranked first (the left panel) and second (the right panel) built from the monomeric constructs representing the most populated cluster from the final production segment of the trajectory. All other top-ranked structures belong to the same structural clusters as these two structures. Residues in the central hydrophobic cluster are shown by their molecular surfaces, hydrophobic Ile32, Val36, and C-terminal Val40 and Ile41 residues are shown in stick representation, with white and blue colors used for different monomers. For Ile32 and Val36 residues transparent molecular surfaces are also shown.

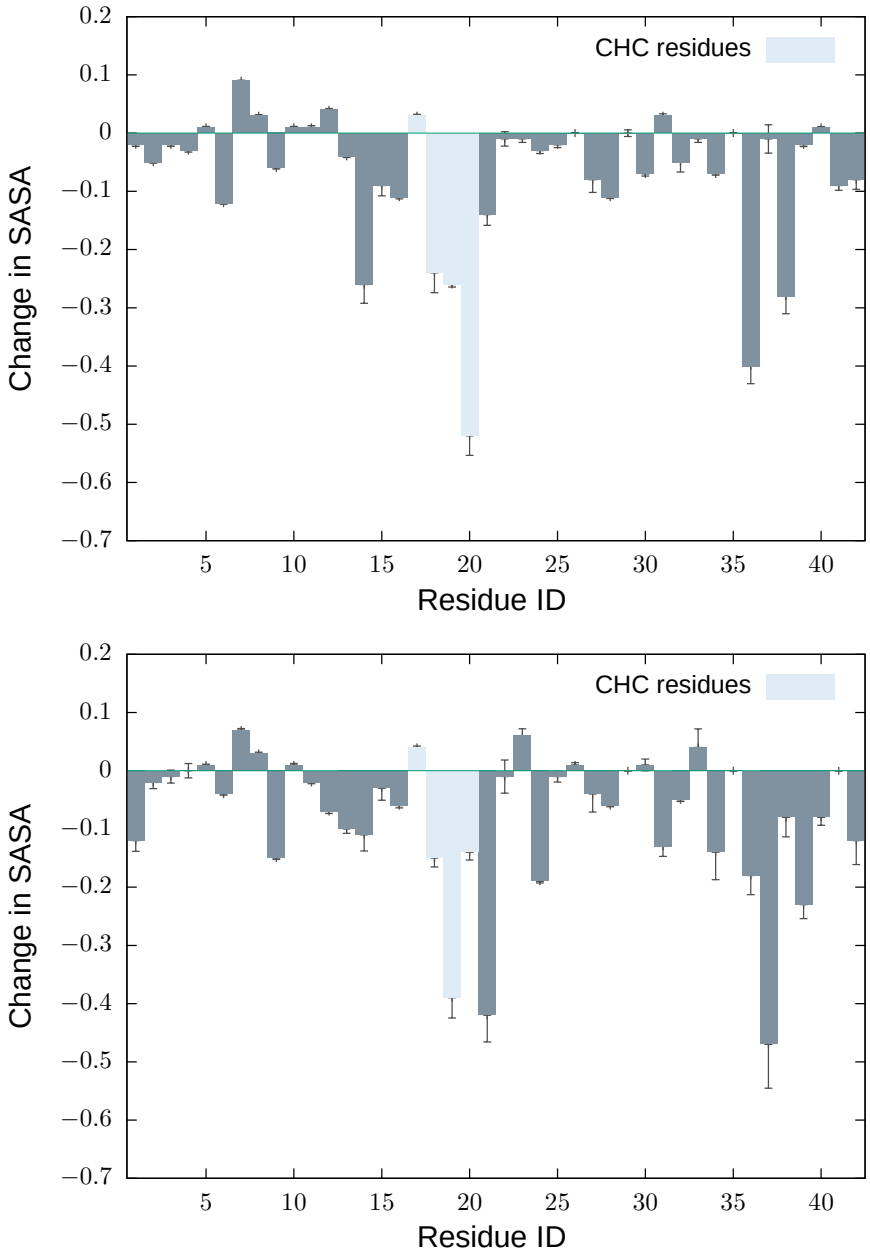

Figure S14: Changes in solvent accessible surface area (SASA) of individual residues upon dimerization of the Aβ42 monomers representing the most populated structural clusters. The top and bottom panels show results for the dimer models built with the monomers from the first and the second production segments of the trajectory, respectively. These monomers have D23-K28 SB in the off state. The SASAs of individual residues are normalized relative to their values in the Gly-X-Gly tripeptide structure in a fully extended conformation. Vertical lines give standard error of means for the ten top-ranked dimer models. Contributions of residues from the CHC domain are shown with a lighter color.

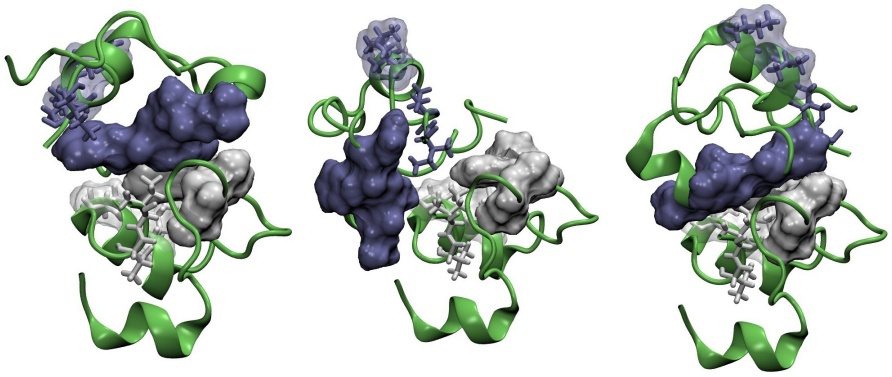

Figure S15: Three top-ranked models of the Aβ42 dimer built from the monomeric constructs representing the most populated cluster and the cluster with a high solvent exposure of hydrophobic residues, both from the first production segment of the trajectory. The same notations are used as in Figure S9.

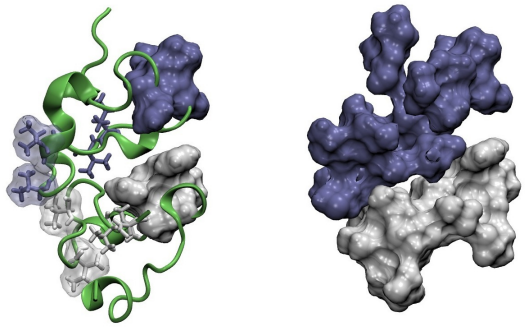

Figure S16: The first-ranked model of the Aβ42 dimer built from the monomeric constructs representing the most populated cluster and the cluster with a high solvent exposure of hydrophobic residues from the last production segment of the trajectory. All three top-ranked structures belong to the same structural cluster. On the left panel, residues in the central hydrophobic cluster are shown by their molecular surface, hydrophobic Ile32 and Val36 residues, as well as C-terminal Val40 and Ile41 are shown in stick representation, with white and blue colors used for different monomers. Transparent molecular surfaces of Ile32 and Val36 are also shown. On the right panel, molecular surfaces of hydrophobic residues (Ala, Leu, Val, Ile, Pro, Phe, Met, Trp) of both monomers are shown with different colors to illustrate shape complementarity of the hydrophobic interface.

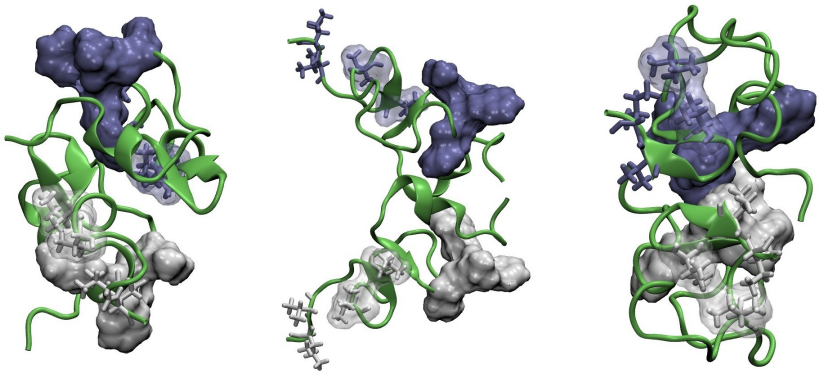

Figure S17: First-ranked models of the Aβ42 dimer built from the different monomeric constructs with β-sheet structure content. Models built with the monomers characterized by a high solvent exposure of hydrophobic residues, and representing the most and least populated clusters are shown in the left, middle, and right panels, respectively. All these monomeric constructs are from the last production segment of the trajectory. The same notations are used as in Figure S9.

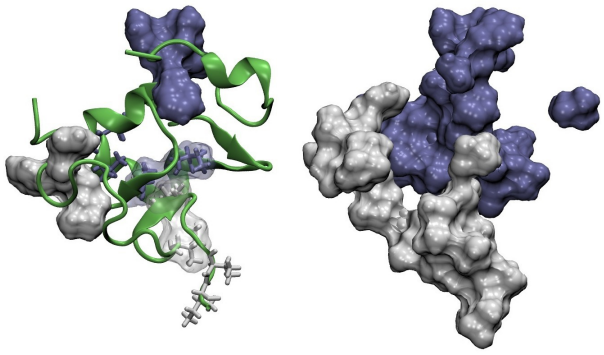

Figure S18: The first-ranked model of the Aβ42 dimer built from the monomeric constructs with β-strand content representing the structural cluster with a high solvent exposure of hydrophobic residues and the most populated cluster. On the left panel, residues in the central hydrophobic cluster are shown by their molecular surface, hydrophobic Ile32 and Val36, as well as C-terminal Val40 and Ile41 residues are shown in stick representation, with white and blue colors used for different monomers. Transparent molecular surfaces of Ile32 and Val36 are also shown. On the right panel molecular surfaces of hydrophobic residues (Ala, Leu, Val, Ile, Pro, Phe, Met, Trp) of both monomers are shown with different colors to illustrate a lack of shape complementarity between hydrophobic patches of two monomers.

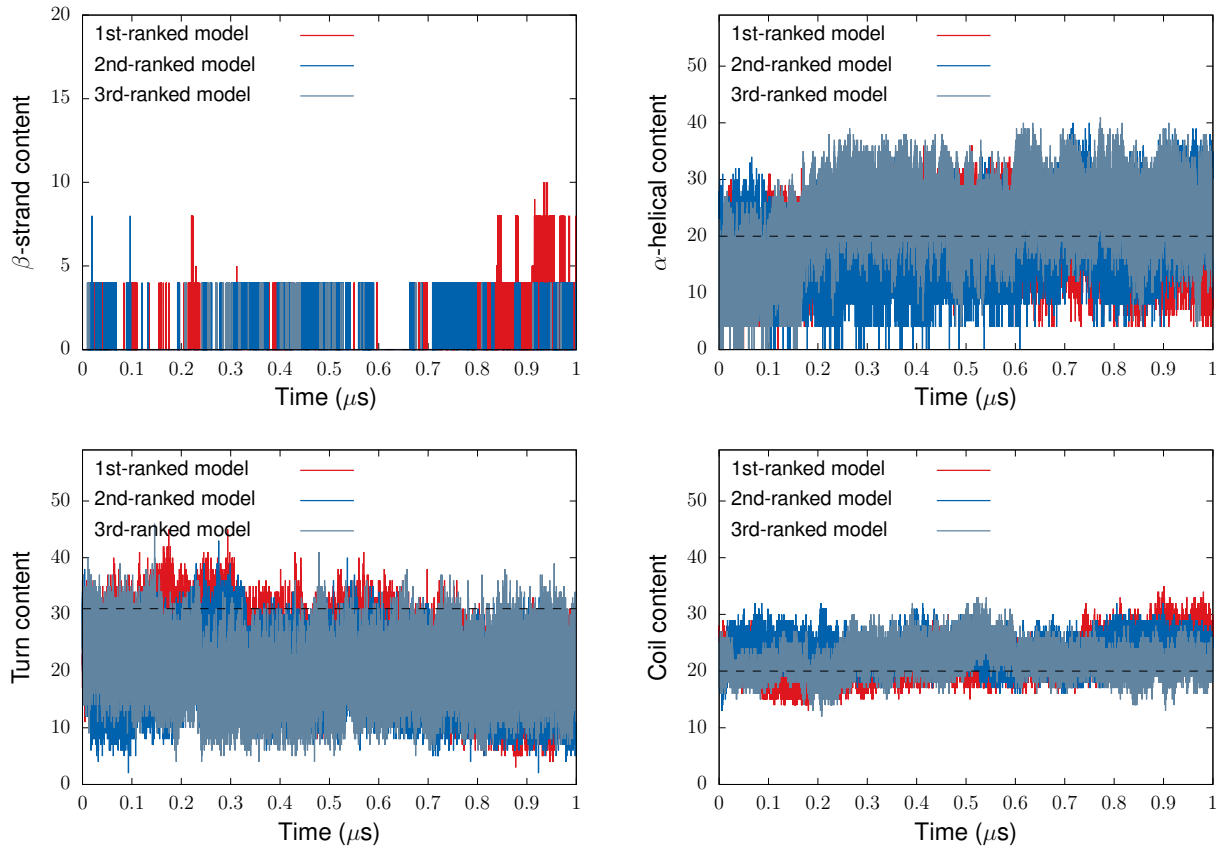

Figure S19: Number of residues involved in different secondary structure elements as a function of simulation time. The dashed horizontal lines show the content for the initial structure. The results are for the Aβ42 dimer model built from the monomers with a large hydrophobic SASA and a disrupted D23-K28 SB.

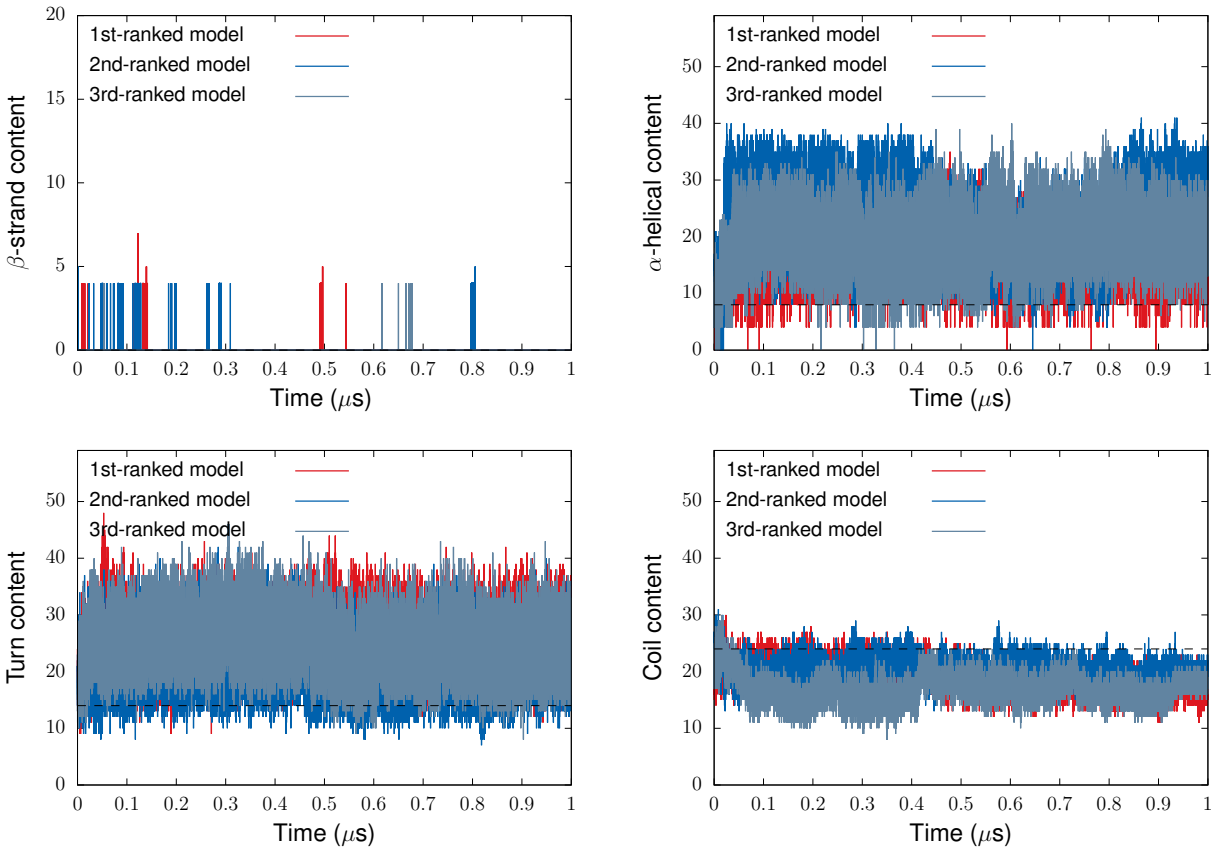

Figure S20: Same as in Figure S19, but for the Aβ42 dimer model built from the monomers with a large hydrophobic SASA and formed D23-K28 SB.

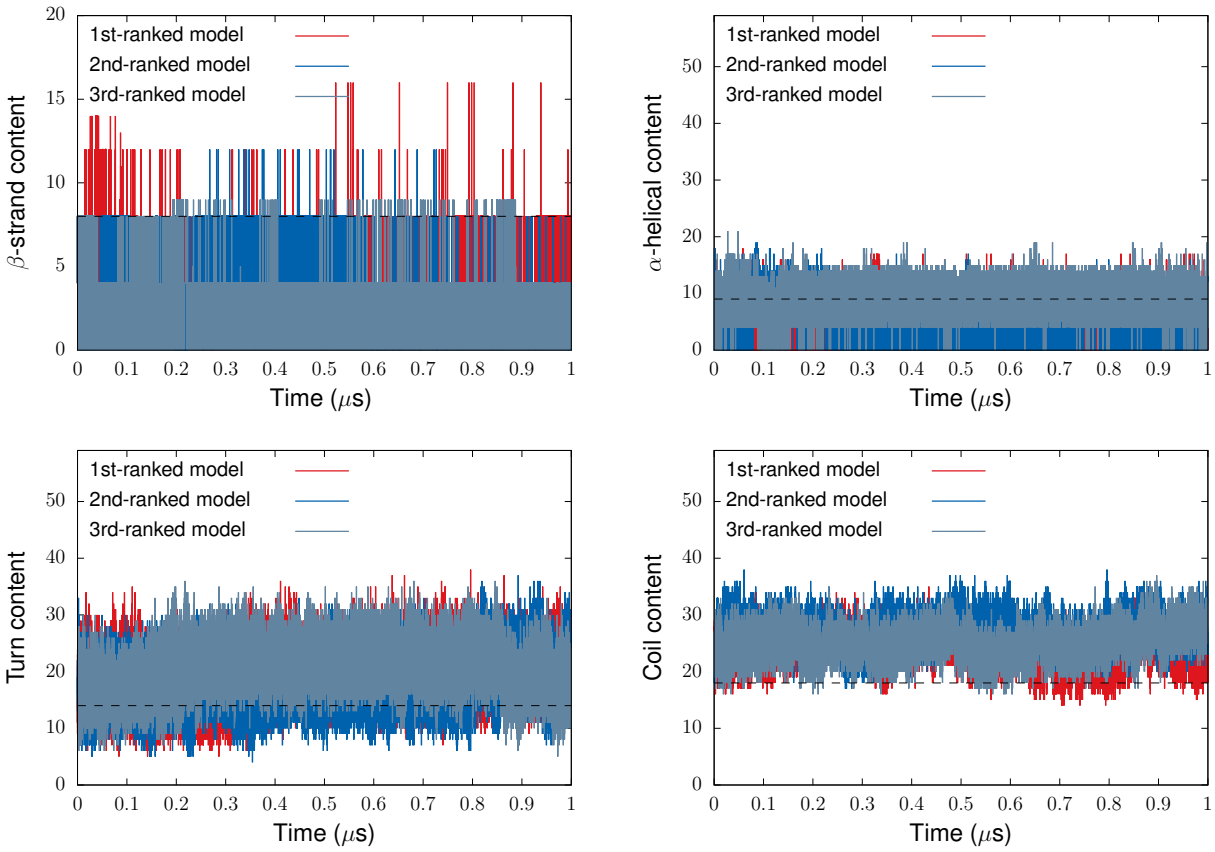

Figure S21: Same as in Figure S19, but for the Aβ42 dimer model built from the monomers with β-sheet structural content.

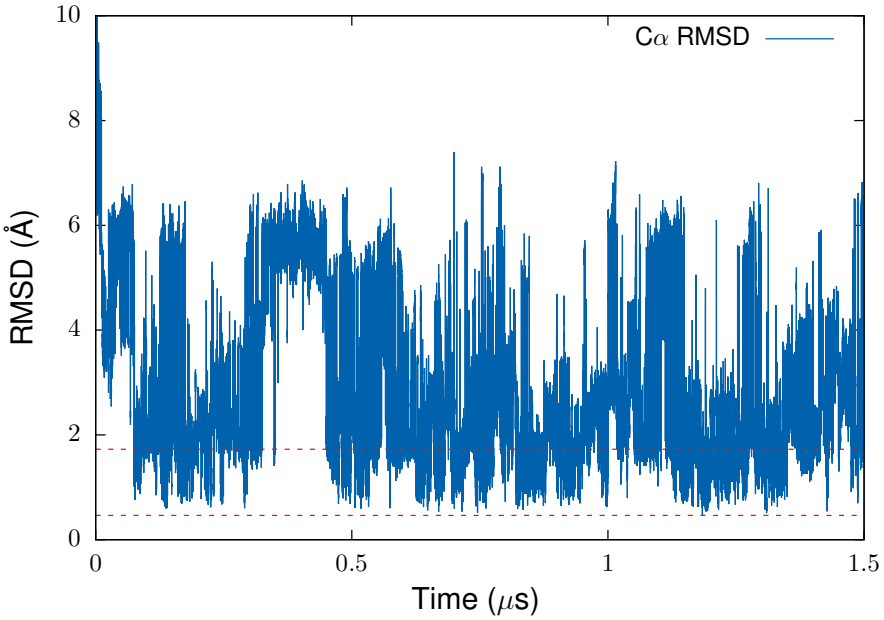

Figure S22: Cα RMSD from REMD folding simulation of the Trp-cage miniprotein starting from a fully extended initial conformation. As a reference structure for the RMSD calculation, the first model of the experimental NMR structure[1] (Protein Data Bank accession code: 1L2Y) was used. The RMSD value of the initial structure is 14.7662 Å. The horizontal dashed lines show the lowest RMSD value of 0.4637 Å (the lower line) and the RMSD value of 1.7258 Å of the conformation representing the most populated structural cluster. Corresponding structures are shown in Figure S23.

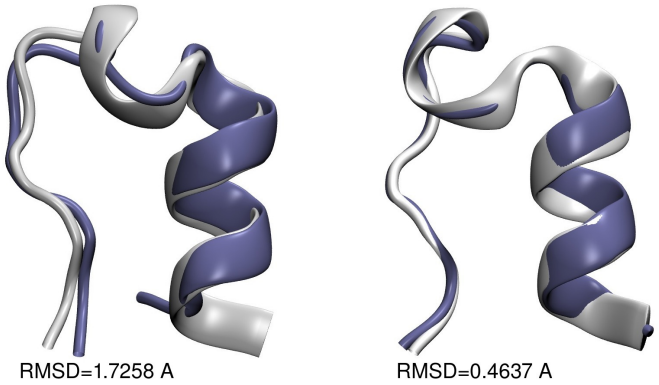

Figure S23: Representative folded structures of the Trp-cage miniprotein[1] from the most populated (the left panel) and the least populated (the right panel) structural clusters identified with clustering the RMSD data shown in Figure S22. For illustration, these structures are superimposed with the experimental model used a reference in the RMSD calculation (shown in white). The structure from the least populated cluster is also characterized by the lowest RMSD value.

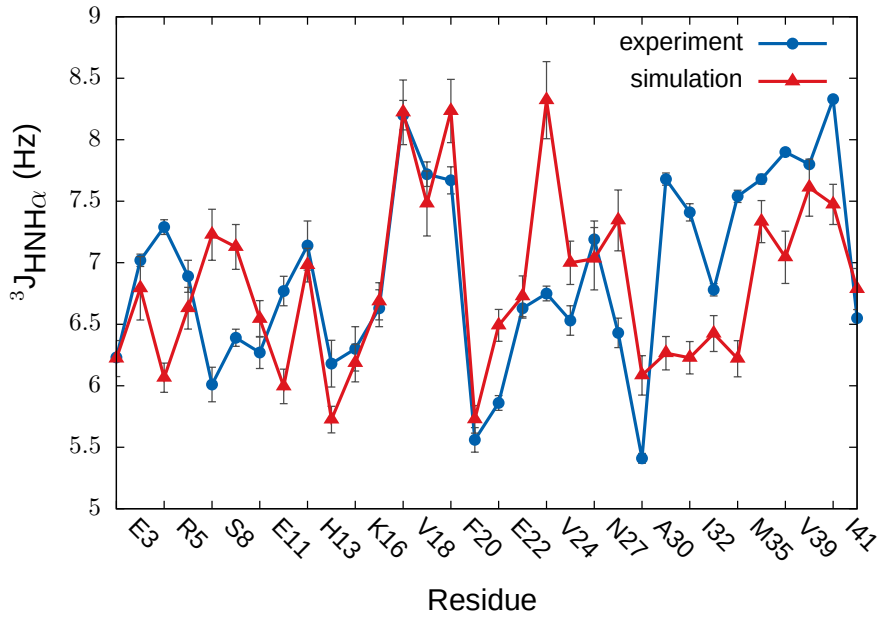

Figure S24: Comparison between calculated and experimental $^3J_{HNH\alpha}$-coupling data. Experimental J-coupling values are from Ref.[2] Only the results corresponding to the reported experimental values are shown. The calculation was performed with the modified Vuister and Bax parametrization[3] of the Karplus equation[4–6] by averaging J-coupling values for individual MD frames corresponding to the large RMSD domain from the last 2μs of the trajectory (see the main text for details). The following values of the Vuister and Bax's parameters were used: Ak = 6.51, Bk = -1.16, and Ck = 1.60.

References

(1) Neidigh, J. W.; Fesinmeyer, R. M.; Andersen, N. H. Designing a 20-residue protein. *Nat. Struct. Mol. Biol.* **2002**, *9*, 425–430.

(2) Roche, J.; Shen, Y.; Lee, J. H.; Ying, J.; Bax, A. Monomeric Aβ1-40 and Aβ1-42 Peptides in Solution Adopt Very Similar Ramachandran Map Distributions That Closely Resemble Random Coil. *Biochemistry* **2016**, *55*, 762–775.

(3) Vuister, G. W.; Bax, A. Quantitative J correlation: a new approach for measuring homonuclear three-bond J($H^N H^\alpha$) coupling constants in ^{15}N-enriched proteins. *Journal of the American Chemical Society* **1993**, *115*, 7772–7777.

(4) Karplus, M. Vicinal Proton Coupling in Nuclear Magnetic Resonance. *Journal of the American Chemical Society* **1963**, *85*, 2870–2871.

(5) Karplus, M. Contact Electron-Spin Coupling of Nuclear Magnetic Moments. *The Journal of Chemical Physics* **1959**, *30*, 11–15.

(6) Karplus, M.; Anderson, D. H. Valence-Bond Interpretation of Electron-Coupled Nuclear Spin Interactions; Application to Methane. *The Journal of Chemical Physics* **1959**, *30*, 6–10.